



Development of variable Mass Effect by Rotary Inertial Damper using a Hydraulic Gear Motor

M. Ikenaga⁽¹⁾, H. Kida⁽²⁾, K. Ikago⁽³⁾, N. Inoue⁽⁴⁾

⁽¹⁾ Assoc. Prof., Kansai University, mikenaga@kansai-u.ac.jp

⁽²⁾ Researcher, Aseismic Devices, CO., LTD, hkida@adc21.co.jp

⁽³⁾ Prof., International Research Institute of Disaster Science, Tohoku University, ikago@irides.tohoku.ac.jp

⁽⁴⁾ Prof., Emeritus, Tohoku University, inoue@archi.tohoku.ac.jp

Abstract

Keywords: Passive Device, Rotary Inertial Damper, Hydraulic Gear Motor, Variable Mass Effect

The seismic devices for severe ground motions are now being developing by many researchers. To satisfy the multiple levels of design criteria under the number of long-period ground motions and severe seismic events, many kinds of devices whose seismic performance changes according to the response displacement and velocity are proposed. These devices control their own damping coefficient by a semi-active mechanism using electricity. Passive devices whose performance changes according to the response without electricity mechanics are also considered as feasibility studies and some devices are already realized. But the passive inertial mass devices whose mass performance changes due to the response have not been seen yet.

The rotary inertial damper using a hydraulic gear motor is developed by Kida and Nakaminami et.al. One of the characteristics of these devices is the simple mechanism of the inertial mass. This damper can control the inertial mass easily by the oil flow. From the previous research, this damper behaves well as the viscous mass damper and the inertial mass effect is much higher than the ordinary viscous mass damper. Authors pay attention to the simple oil flow which can control the inertial mass with the hydraulic gear motor, and small- scaled damper for rotary inertial damper with variable mass effect is developed. To realize the variable inertial mass effect, two oil flow paths are applied and oil flow is controlled according to the damper deformation.

Numbers of dynamic sinusoidal experiments are conducted to check the behavior of this damper. From the test results, three points of conclusions are obtained. (1) From the results of damper whose performance is not changed, it is shown that this prototype damper can control the oil flow by on-off valves and behaves as an ordinary viscous damper a viscous mass damper. (2) The sinusoidal experiments using the damper whose performance is changed at the defined displacement, indicate that both the inerter mass performance and the viscous damping performance increase. (3) From the time history analysis of the damper, the hysteresis loop and the behavior of changing performance on the inerter mass can be simulated in the good accuracy.



1. Introduction

Seismic devices whose damping performance changes due to the input ground motions are now developing by many researchers. To satisfy the multiple levels of design criteria under numbers of seismic excitations with a wide range of characteristics from long-period ground motions to pulse motions, variable performance devices are focused on as one of the solutions. Active or semi-active devices are typical variable devices, such as an actuator or a magnet-rheological fluid damper [1]. On the other hand, several researchers suggest the powerless devices that control the seismic damping performance passively by the mechanism.

Tabei and Inoue et al. [2] and Nemoto et al [3] developed a variable oil damper whose damping performance changes due to the damper displacement. The analytical study shows that the variable damping performance can improve the performance of seismic protection compared to the ordinary oil damper. Maseki et al. [4] developed another type of variable oil damper controlled by the displacement and show the possibility of response control for seismic isolated buildings analytically and experimentally. The characteristics of these dampers are passive control powerless devices for oil dampers. Hori and Inoue et al. [5] proposed the friction damper with coupling mechanism and Ikenaga et al. [6] show the advantages of that analytically. This damper activates the friction element when the damper displacement becomes larger than the set displacement by the mechanical engagement. Researches on variable damping or stiffness are as described above, but researches of variable performance on inerter can be found in the range of passive devices.

Wang et al. [7] proposed the generated rotor (hereinafter denoted as gerotor) attached to the flywheel to realize an amplified inertance. Kida and Nakaminami et al. [7],[8],[9] developed this concept to the real scaled damper named inertial hydraulic gerotor damper (hereinafter denoted as iHGD) and experimentally represented the performance of gerotor. In these papers, authors note that iHGD can design the damper mechanism easily by the relationships of oil flow to a gerotor. They also suggested the concept of the variable inertial mass system using an iHGD.

In this paper, we developed a small-scaled inertial hydraulic gerotor damper with variable inertance, and carried out dynamic sinusoidal experiments to know the behavior of inertance variation.

2. Inertial Hydraulic damper using a hydraulic gear motor with variable mass effect

Figure 1 and 2 shows the diagram and drawing of iHGD with variable inertance. The fluid flow of Bypass A produces the rotational motion of the gerotor. This iHGD consists of a cylinder, a piston with a rod, a bypass A that a gerotor with a flywheel is installed, and a bypass B. The hydraulic fluid that flows into the gerotor rotates the two gears in the casing, thereby generating torque about its rotary shaft.

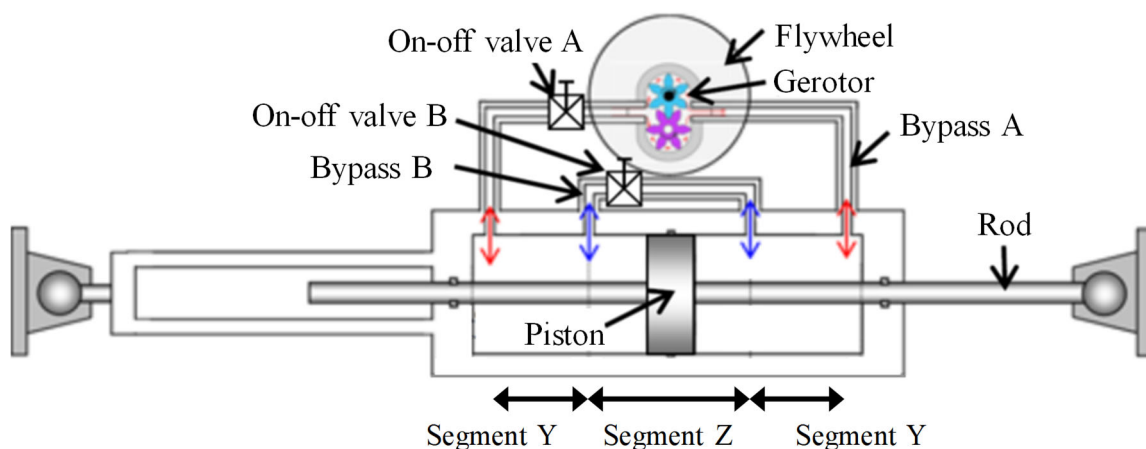


Fig. 1 – Diagram of iHGD with variable inertance

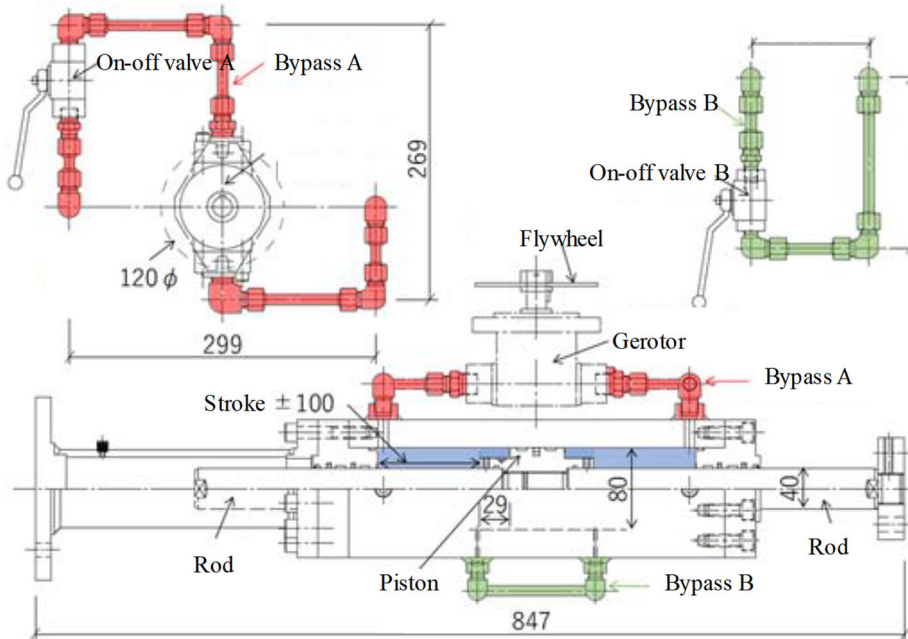


Fig. 2 – Inertial hydraulic gerotor damper (iHGD) with variable inertia

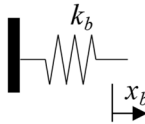
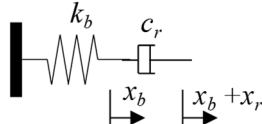
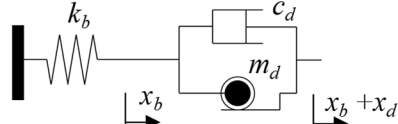
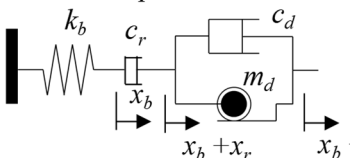
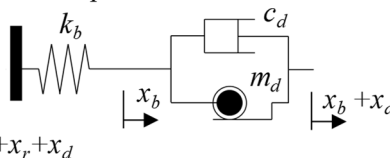
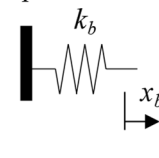
Table 1 lists the specification of iHGD with variable mass effect. The displacement volume required to allow rotation of the shaft by one turn is denoted by V_m (mm^3/rev). When the piston moves, the fluid flows through the bypass tube and the gerotor casts both the viscous damping force and the inertial resisting force. The calculated inertia is 8.9 tons, which the amplification factor of gerotor for physical mass is 33400 times. The hydraulic fluid flows of bypass A and B can be controlled with the on-off valve A and B. Table 2 represents the six kinds of the state which are determined from the piston position and the on-off valve status. Analysis models corresponding to six kinds of state are also illustrated in Table 2.

Table 1 – Specimen specifications

	Notation	Unit	Value
Pressure receiving area	A_p	mm^2	3770
Displacement volume	V_m	mm^3/rev	5500
Displacement of piston per rotation	x_m	mm	1.46
Cross section area of bypass A tube	A_e	mm^2	38.5
Length of bypass A tube	l	mm	910
Cross section area of bypass B tube	A_{be}	mm^2	38.5
Length of bypass B tube	l_b	mm	520
Density of hydraulic oil (15 °C)	ρ	ton/m^3	0.871
Ratio of cross section area	α		98
Diameter	D_0	mm	120
Thickness	t	mm	3
Flywheel			
Physical mass	m_0	ton	0.00026634
Inertance	m_{d1}	ton	8.9
Fluid inertance of bypass A	m_{d2A}	ton	0.29
Fluid inertance of bypass B	m_{d2B}	ton	0.17
Allowable pressure	p_{\max}	Mpa	21
Allowable rotational speed	n_{\max}	rpm	4000
Allowable maximum force	F_{\max}	kN	79.2
Allowable velocity	$x_{d\max}$	mm/s	97.3



Table 2 – Analysis models of iHGD under six conditions of the piston and the on-off valve

	State 1	State 2	State 3
Position of piston	Segment Z	Segment Z	Segment Z
On-off valve A	Close	Close	Open
On-off valve B	Close	Open	Close
Analysis model			
	State 4	State 5	State 6
Position of piston	Segment Z	Segment Y	Segment Y
On-off valve A	Open	Open	Close
On-off valve B	Open	Open or Close	Open or Close
Analysis model			

where F_d , k_b , c_r , m_d and c_d represent the reaction force of the iHGD, the stiffness of the damper includes the oil fluid elasticity, the damping coefficient of the oil fluid in bypass B, the inertance of the flywheel and oil fluid in bypass A, and the damping coefficient of the oil fluid in bypass A respectively. While x , x_b , x_r , x_d is the displacement of the piston, the displacement that divided the fluid flow volume in bypass B by the area of bypass B, and the displacement that divided the fluid flow volume in bypass A by the area of bypass A, respectively. When the on-off valve A is closed, the oil fluid does not pass through the bypass A so that the gerotor and flywheel are never activated (state 1, 2, and 6). The bypass B is activated only when the on-off valve B is open and the position of the piston is in range of segment Z (state 2 and 4). The analysis model of state 2 is the same as the Maxwell model because of the damper stiffness and the oil flow in bypass B, while those of state 3 and 5 are the same as the viscous mass damper because of the bypass A and gerotor. In case the position of the piston is in range of segment Z and both on-off valves are opened, the oil fluid passes through both bypass illustrated as state 4. It is noted that the pressure in the bypass A and B is equal so that the reaction force can be described as follows;

$$F_d = k_b x_b = c_r \dot{x}_r = c_d \dot{x}_d + m_d \ddot{x}_d \quad (1)$$

$$x = x_b + x_r + x_d \quad (2)$$

3. Experiment Outline

Figure 3 shows the experimental setup and figure 4 shows the photograph of iHGD. The dynamic loading examinations are carried out by the dynamic actuator that is controlled by the displacement. The maximum reaction force, maximum loading speed, and maximum amplitude of the actuator are $\pm 50\text{kN}$, $\pm 0.75\text{m/s}$, and $\pm 400\text{mm}$ respectively. The actuator is attached to the iHGD through the rubber plates as the buffer (herein after called “a rubber unit”). Sine waves with the anteroposterior taper whose frequency is in range of 0.1Hz to 1.0Hz and the amplitude is in range of 10mm to 60mm. The measurement data are the displacement of iHGD specimen, that of the rubber unit, that of the summation of iHGD specimen and the rubber unit which is approximately equal to the actuator displacement, the temperature of the bypass A and B, and the reaction force from the loadcell attached to the actuator.

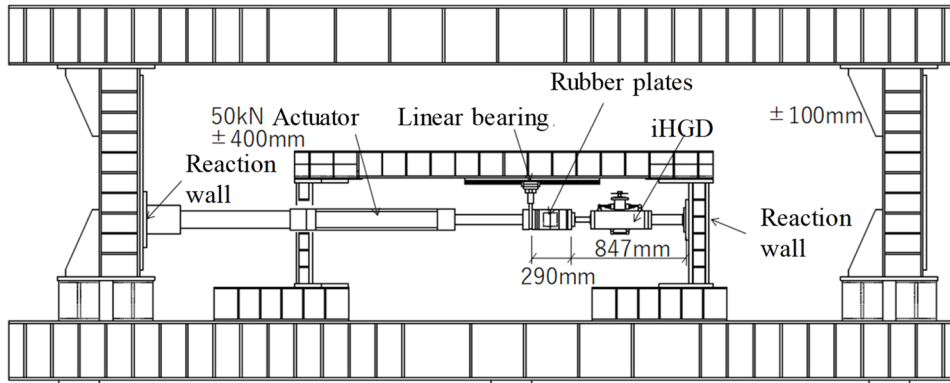


Fig. 3 – Diagram of experimental setup

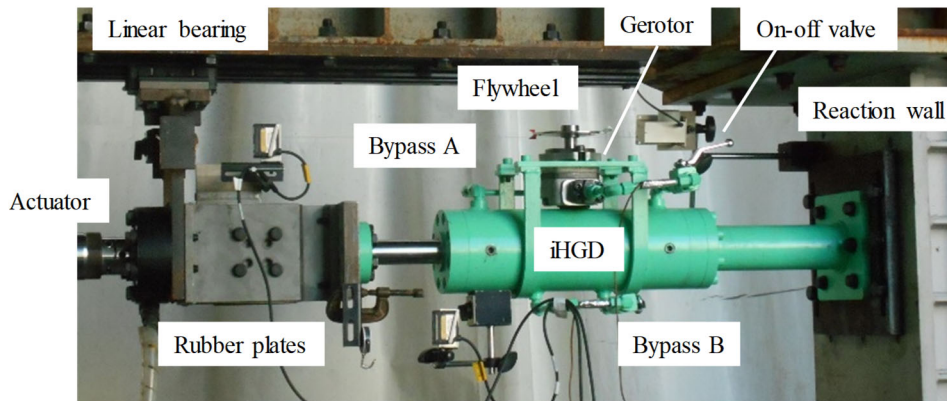


Fig. 4 – Photograph of iHGD with variable inertia and experimental setup

First of all, the stiffness of the rubber unit and loading frame is investigated to refer to in the following studies. To eliminate the damping force and the inertia effect, on-off valve A and B are closed (analysis model state 1) and sine wave loadings are conducted. Figure 5 represents the loading experiment results. From the hysteresis loops, it is clear that both behaviors can be considered as almost linear. The stiffness of the rubber unit k_g is 1.32 kN/mm and the stiffness of the reaction frame k_f is 29.6 kN/mm. The damper stiffness k_b is also determined to be 20 kN/mm from the relationship between the reaction force F_d and the damper displacement x_b . Note that the stiffness k_b in analysis is calculated assuming k_g and k_b are connected in series.

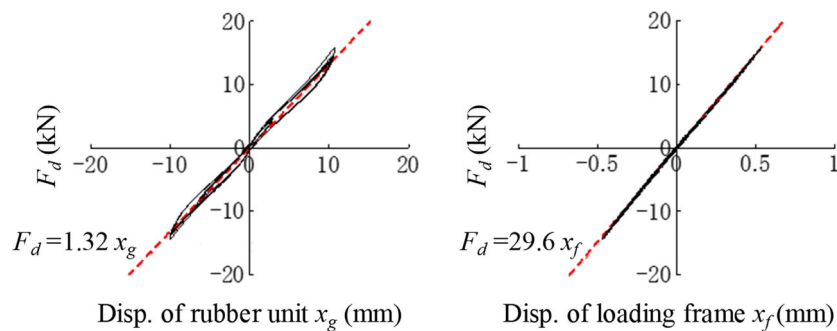


Fig. 5 – Hysteresis loops for displacement of rubber unit and loading frame



4. Experiment Result

Figure 6 (a) and (b) show the hysteresis loop examples under state 2 with rubber unit. Figure 6 (c) plots the relationship between the maximum velocity of bypass B and the maximum reaction force Q_{vr} . From table 2 it is shown that the reaction force F_d is equal to the damping force of bypass B dashpot under the state 2. From the hysteresis loop, the iHGD behaves as the viscous damper when the on-off valve A is closed. The coefficient c_r has nonlinearity to the velocity and is obtained as follows:

$$c_r = 0.0163 \times |\dot{x}_r|^{0.5} \quad (3)$$

From the obtained c_r and analysis model in table 2, the numerical time history analysis is conducted. Figure 6 (b) describes the hysteresis loops of experimental result and analysis result that the measured displacement of the actuator is applied to the input displacement. Both results are in good agreement.

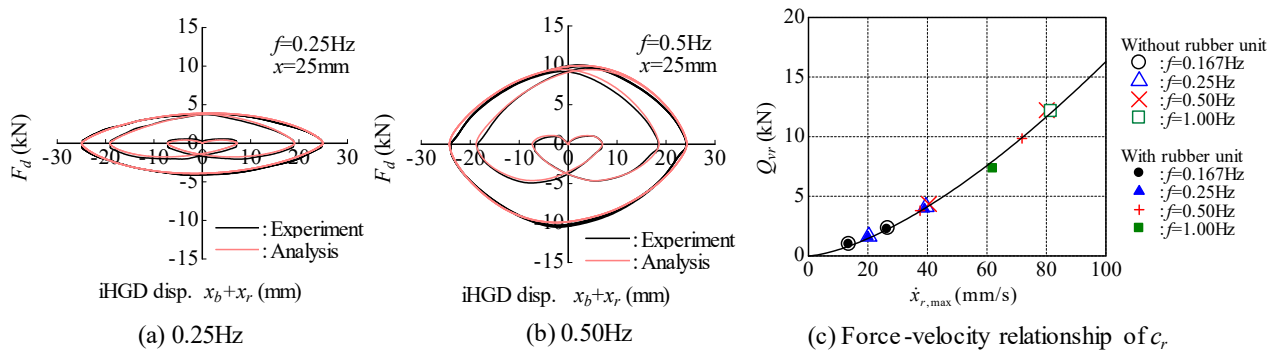


Fig. 6 Hysteresis loops and force-velocity relationship of iHGD under state 2 ($x=25\text{mm}$)

Figure 7 (a) and (b) show the hysteresis loop examples under the state 3 and 5 with rubber unit. Figure 7 (c) plots the relationship between the maximum velocity of bypass A and the maximum reaction force Q_{vd} . The reaction force F_d is equal to the sum of the damping force of bypass A and the inertial force of the flywheel. From figure 7, it is known that a gap of approximately 1 mm is found at the left and right ends of each hysteresis loop. It is probably due to the internal air in bypass A that is attached to the upper part of iHGD. The hysteresis shown in figure 7 (a) and (b) is skewed clockwise due to the inertance of the fluid in bypass A and the gerotor. The amount of inertance is approximately 11.5 tons. From table 2 the assumed inertance is 8.9 tons so that it is considered that the inertance is affected by the gerotor parts and volumetric efficiency. The coefficient c_d also has nonlinearity to the velocity and is obtained as follows:

$$c_d = 0.775 \times |\dot{x}_d|^{-0.357} \quad (4)$$

Figure 7 (b) describes the hysteresis loops of the experimental result and analysis result of iHGD under status 3 and 5. In the analysis model, the gap behavior is considered as the retrograde type stiffness of k_b . The analysis result can simulate the experimental result well.

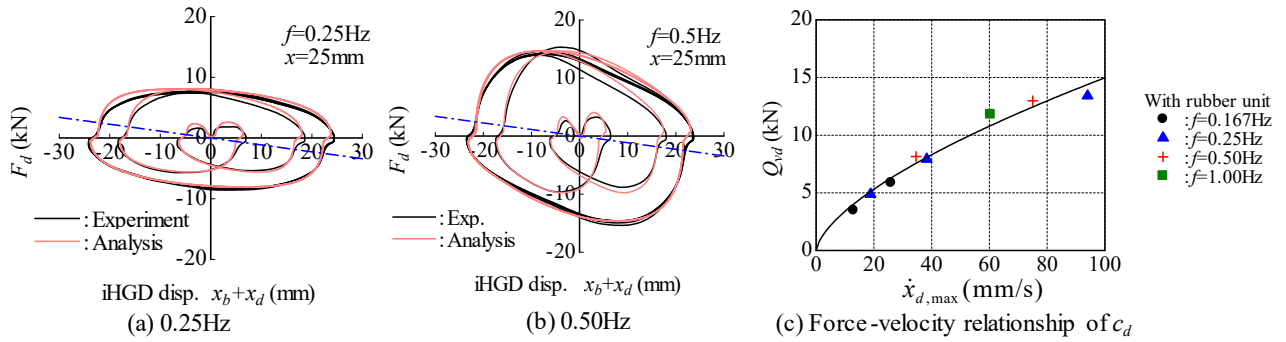


Fig. 7 - Hysteresis loops and force-velocity relationship of iHGD under state 3 ($x=25\text{mm}$)

Figure 8 (a) and (b) shows the hysteresis loops under the state 4 with rubber unit. In these cases, both on-off valves are open but the displacement is 25 mm so that bypass A and B are activated. The reaction force of iHGD under state 4 is smaller than that under state 3 in the same loading condition. It is because state 4 is obtained by connecting state 2 and state 3 in series. The parameters for this analysis refer to the data described above. The analysis results are in good agreement with the experimental result.

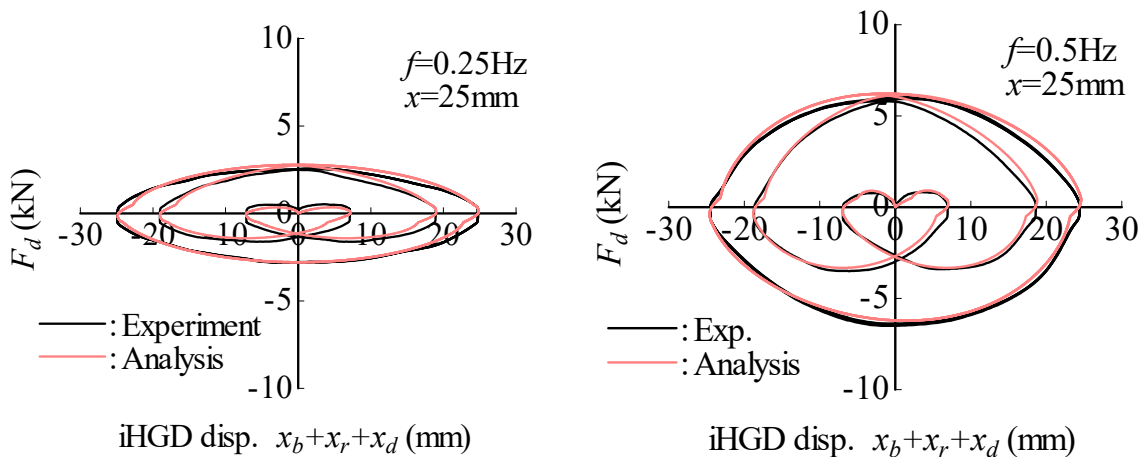


Fig. 8 - Hysteresis loops and force-velocity relationship of iHGD under state 4 ($x=25\text{mm}$)

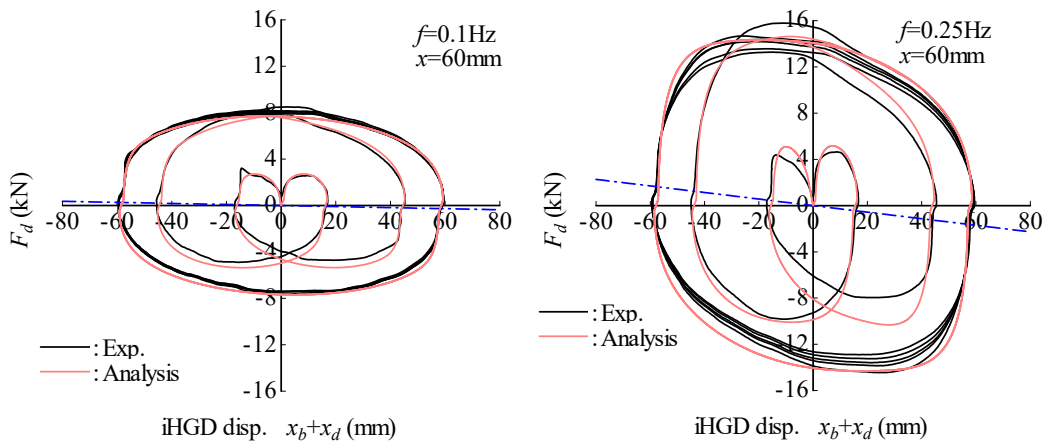


Fig.9 - Hysteresis loops and force-velocity relationship when only the on-off valve A is open



Figure 9 shows the hysteresis loops when the on-off valve B is closed. The range of displacement is from -60mm to 60 mm and the position of the piston moves from segment Z to segment Y, but the damper performance keeps constant because the fluid flow never goes through in bypass B when the on-off valve B is closed. The obtained inertance of iHGD from these hysteresis loops are the same as that in figure 7.

Figure 10 shows the hysteresis loops when the on-off valve A and B are open. Both the bypass A and B are activated when the displacement is within 30 mm. After that the piston starts to close the entrance of bypass B and the whole area of bypass B will be closed when the displacement achieves to approximately 40mm. Referring to table 2, the model of iHGD is state 4 within the displacement of ± 30 mm and the model change to state 5 in the range over ± 40 mm displacement. In the analysis, the analysis model state 4 is applied at first and analysis model changes to state 5 when the absolute displacement exceeds 40 mm. The behavior of the hysteresis loop of the experimental result shows that the reaction force soars when the displacement exceeds 40 mm. When the displacement is within 40 mm, analysis results and experimental results are in good agreement. But the reaction force of the analysis result becomes larger than that of the experimental result after the state change from 4 to 5. The time histories of the reaction force under 0.25Hz loading depicted in figure 11 shows that the analysis result overestimates the maximum reaction force of the experimental result. It is considered that the difference of the maximum force is due to the air inside the bypass A or some fluid flow effect.

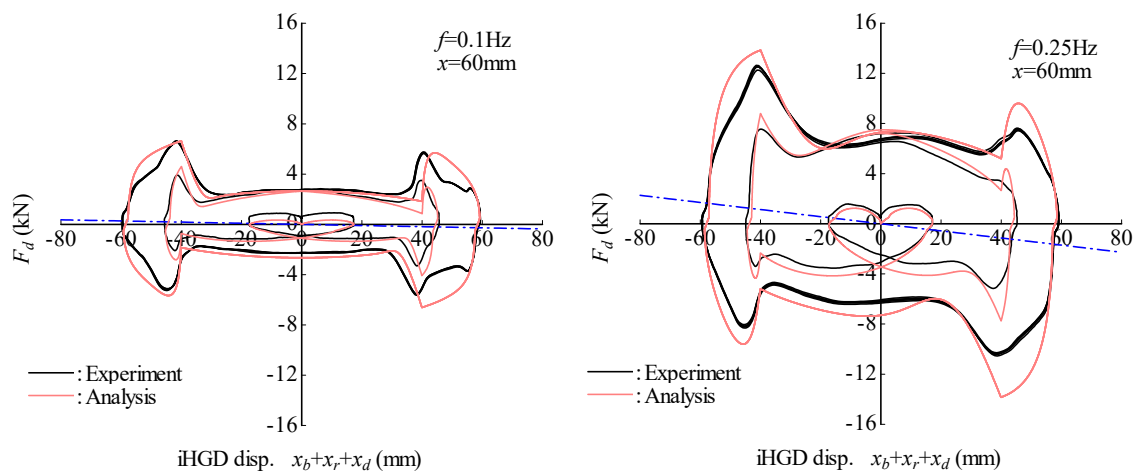


Fig.10 - Hysteresis loops and force-velocity relationship when the on-off valve A and B are open

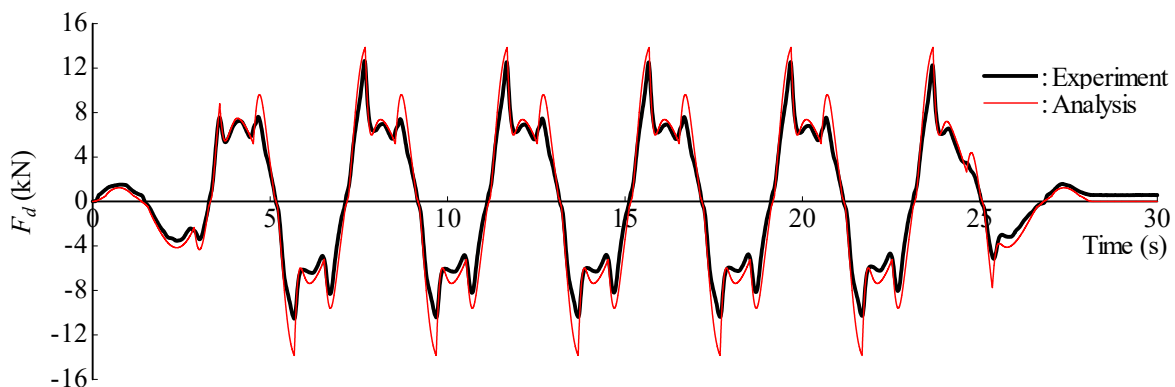


Fig.11 – Time history of reaction force under 60 mm amplitude sine wave (On-off valve A and B are open)



4. Conclusion

This paper has discussed the feasibility study on an iHGD with variable inertance mechanism without any external power supply by two bypasses of the fluid flow. Sinusoidal experimental results revealed the performance of the suggested damper and the inertance variation could be realized using this damper. The six simulation analysis models corresponding to the damper setup and range of the displacement are proposed and the analysis results are generally in good agreement with the experimental results. Further studies are necessary for the reaction force estimation after the inertance performance is changed.

5. Acknowledgements

The writers are grateful for the production support of the test specimen from Oxjack co.,ltd and Nakamura Techno Service.

6. References

- [1] Ikenaga, M., M., Ikago, K., Inoue, N. (2011): Seismic displacement control design of base isolated structures by MR dampers based on pseudo complex damping control rules. *Proceedings of the 13th International Conference on Civil Structural and Environmental Engineering Computing*, paper 69.
- [2] Tabei, N., Hori, N., Inoue, N. (2009): Development of variable oil damper and its application for seismic isolation structures. *Journal of Structural and Construction Engineering (Transactions of AIJ)*, 74(636), 259–266.
- [3] Nemoto, M., Ikenaga, M., Ikago, K., Inoue, N. (2011): A Design Method of a Base Isolated System for Detached Houses Using Variable Oil Dampers. *Journal of Structural and Construction Engineering (Transactions of AIJ)* 76(660), 291-299.
- [4] Maseki, R., Nagashima, I., Nii, A., Kimura, Y., Nishitani, A. (2015): Response Control of Seismic Isolated Buildings Using Developed Passive-Switching Oil Damper with Bi-Flow Mechanism. *Journal of Structural and Construction Engineering (Transactions of AIJ)*, 80(713), 1023-1032.
- [5] Hori, N., Zhao, Z., Mateo, A., Inoue, N. (2009): Control of Seismic Response Displacement of Base Isolated Structure Specimen by Friction Damper with Joint Mechanism : Part 1, part2. *Summaries of Technical Paper of Annual Meeting of AIJ*, Structure II, 885-888.
- [6] Ikenaga, M., Fukumi, Y., Ikago, K., Inoue, N. (2013): Application of Friction Damper with Coupling Mechanism Designed in Accordance with Input Ground Motion Levels to a Base Isolated Detached House. *Journal of Structural and Construction Engineering (Transactions of AIJ)* 78(690), 1413-1422.
- [7] Kida, H., Nakaminami, S., Ikago, K., Inoue, N. (2017): Development of a Rotary Inerter Damper using a Hydraulic Gear Motor, Part1, part2. *Summaries of Technical Paper of Annual Meeting of AIJ*, Structure II, 631-634.
- [8] Nakaminami, S., Kida, H., Ikago, K., Inoue, N. (2018): Development of a Rotary Inerter Damper using a Hydraulic Gear Motor, Part3, part4. *Summaries of Technical Paper of Annual Meeting of AIJ*, Structure II, 453-456.
- [9] Nakaminami, S., Kida, H., Ikago, K., Inoue, N. (2017): Dynamic testing of a Full-scale Hydraulic Inerter-Damper for the Seismic Protection of Civil Structures, *Proceedings of the 7th International Conference on Advances in Experimental Structural Engineering*, Pavia, Italy, 57-79.